The E3 ubiquitin ligase Mule acts through the ATM–p53 axis to maintain B lymphocyte homeostasis

Zhenyue Hao,[1,2,3] Gordon S. Duncan,[1] Yu-Wen Su,[1] Wanda Y. Li,[1] Jennifer Silvester,[1] Claire Hong,[1] Han You,[1] Dirk Brenner,[1] Chiara Gorrini,[1] Jillian Haight,[1] Andrew Wakeham,[1] Annick You-Ten,[1] Susan McCracken,[1] Andrew Elia,[1] Qinxi Li,[1] Jacqui Detmar,[5] Andrea Jurisicova,[5] Elias Hobeika,[6,7] Michael Reth,[6,7] Yi Sheng,[8] Philipp A. Lang,[1] Pamela S. Ohashi,[1,2,3,4] Qing Zhong,[9] Xiaodong Wang,[10] and Tak W. Mak[1,2,3,4]

[1]The Campbell Family Institute for Cancer Research and [2]Ontario Cancer Institute, University Health Network, Toronto, Ontario M5G 2M9, Canada
[3]Department of Medical Biophysics and [4]Department of Immunology, University of Toronto, Toronto, Ontario M5G 2C1, Canada
[5]Division of Reproductive Sciences, Department of Obstetrics and Gynecology, Samuel Lunenfeld Research Institute, Mount Sinai Hospital, Toronto, Ontario, M5G 1X5, Canada
[6]Max Planck Institute of Immunobiology and [7]Centre for Biological Signaling Studies, BIOSS, University of Freiburg, 79104 Freiburg, Germany
[8]Department of Biology, York University, Toronto, Ontario M3J 1P3, Canada
[9]Division of Biochemistry and Molecular Biology, Department of Molecular and Cell Biology, University of California, Berkeley, CA 94720
[10]Howard Hughes Medical Institute and Department of Biochemistry, University of Texas Southwestern Medical Center at Dallas, Dallas, TX 75390

Cellular homeostasis is controlled by pathways that balance cell death with survival. Mcl-1 ubiquitin ligase E3 (Mule) is an E3 ubiquitin ligase that targets the proapoptotic molecule p53 for polyubiquitination and degradation. To elucidate the role of Mule in B lymphocyte homeostasis, B cell–specific *Mule* knockout (BMKO) mice were generated using the Cre–*LoxP* recombination system. Analysis of BMKO mice showed that Mule was essential for B cell development, proliferation, homeostasis, and humoral immune responses. p53 transactivation was increased by two- to fourfold in Mule-deficient B cells at steady state. Genetic ablation of p53 in BMKO mice restored B cell development, proliferation, and homeostasis. p53 protein was increased in resting Mule-deficient mouse embryonic fibroblasts (MEFs) and embryonic stem (ES) cells. Loss of Mule in both MEFs and B cells at steady state resulted in increased levels of phospho–ataxia telangiectasia mutated (ATM) and the ATM substrate p53. Under genotoxic stress, BMKO B cells were resistant to apoptosis, and control MEFs exhibited evidence of a physical interaction between Mule and phospho-ATM. Phospho-ATM, phospho-p53, and Brca1 levels were reduced in Mule-deficient B cells and MEFs subjected to genotoxic stress. Thus, Mule regulates the ATM–p53 axis to maintain B cell homeostasis under both steady-state and stress conditions.

CORRESPONDENCE
Zhenyue Hao:
zhenyuehao@gmail.com
OR
Tak. W. Mak:
tmak@uhnres.utoronto.ca

Abbreviations used: Ab, antibody; ATM, ataxia telangiectasia mutated; BDKO, B cell–specific double KO; BMKO, B cell–specific *Mule* KO; CSR, class switch recombination; Dox, doxorubicin; ES, embryonic stem; FO, follicular; MEF, mouse embryonic fibroblast; Mule, Mcl-1 ubiquitin ligase E3; MZ, marginal zone; $NP_{(15)}$-CG, 4-hydroxy-3-nitrophenylacetyl–chicken γ-globulin; Td, T dependent; Ti, T independent; TS, transitional; VSV, vesicular stomatitis virus.

The homeostasis of any cellular compartment is maintained by complex pathways that balance survival and apoptosis. For lymphocytes, prosurvival signaling pathways are often countered by the intrinsic pathway of apoptosis in the mitochondria (Rathmell and Thompson, 2002), such that mutation of genes in this pathway leads to lymphoproliferative disorders (Bouillet et al., 1999; Rathmell et al., 2002; Hao et al., 2005). Mitochondrial apoptosis can be triggered by the activation of p53, a major regulator of cellular homeostasis under both steady-state and stress conditions (Villunger et al., 2003; Green and Kroemer, 2009). Because indiscriminant triggering of p53 activation could kill healthy

The Rockefeller University Press $30.00
J. Exp. Med. Vol. 209 No. 1 173-186
www.jem.org/cgi/doi/10.1084/jem.20111363

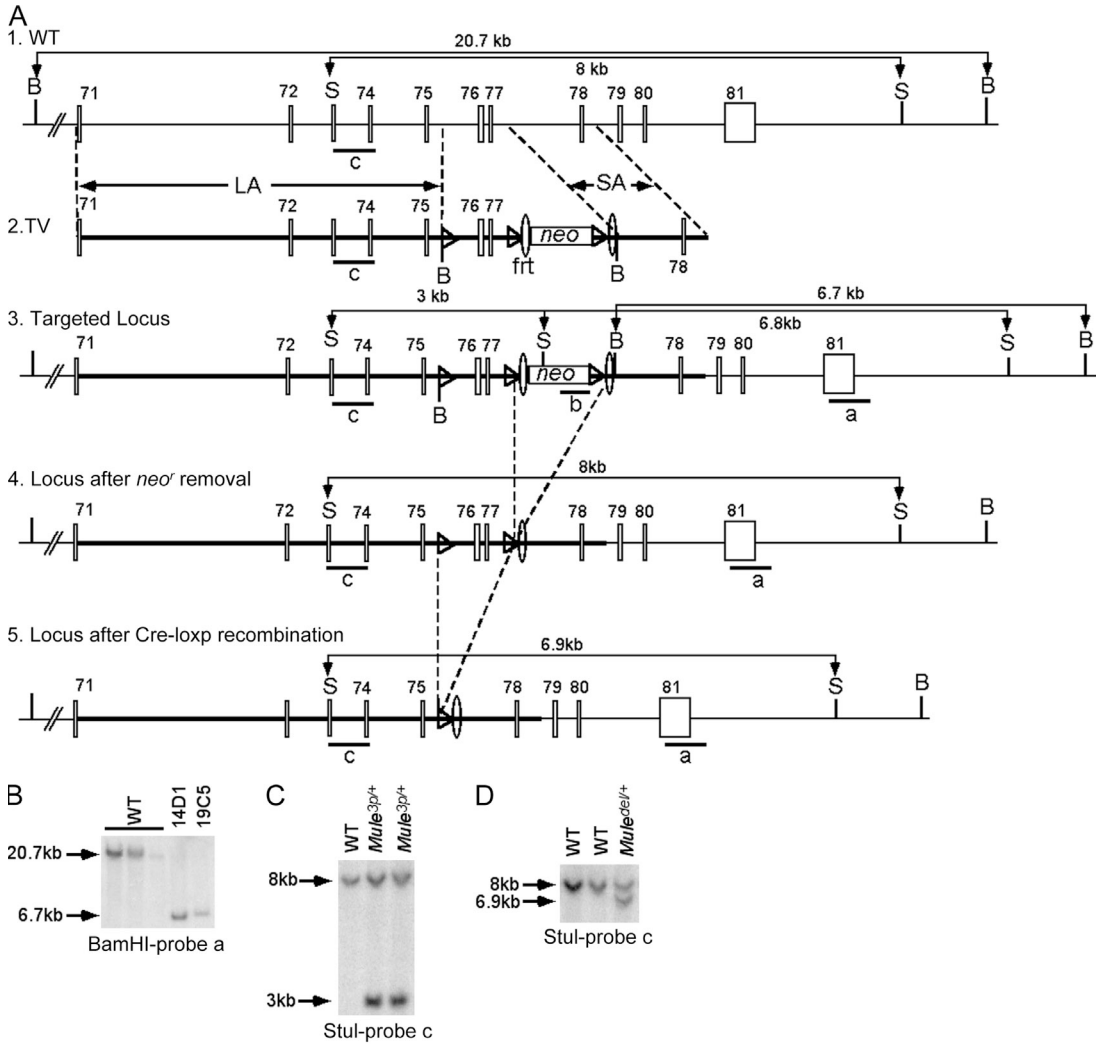

Figure 1. Generation of floxed *Mule* mice. (A) Targeting scheme. (1) Restriction map of the WT genomic mouse *Mule* locus. Probes used to verify targeting events are indicated as a, b, and c. The expected sizes of the restriction fragments are shown. B, BamHI; S, StuI. (2) Targeting vector (TV) construction. The *loxP*-flanked neomycin resistance gene (neo) was used as a selection marker during ES cell culture. Exons 76 and 77, which encode the HECT domain essential for Mule's E3 ubiquitin ligase activity, were flanked by *loxP* sites (triangles). (3–5) The structure of the targeted *Mule* locus (3), the targeted locus after removal of neo (4), and the locus after deletion of the floxed exons (5) are shown, including the sizes of diagnostic restriction fragments. (B) Southern blot analysis of ES cell clones. Genomic DNA from WT E14K cells and two mutant clones (14D1 and 19C5) were digested with BamHI and hybridized with probe (a) to verify the targeting event. (C) Southern blot analysis of genomic DNA from agouti mice carrying the WT or targeting allele ($Mule^{3P/+}$) as indicated in A3. DNA was digested with StuI and hybridized with probe c to verify germline transmission. (D) Southern blot analysis of genomic DNA from mice carrying the deleted *Mule* allele ($Mule^{del/+}$) as indicated in A5. DNA was digested with StuI and hybridized with probe c.

cells and thus disrupt homeostasis, p53 protein stability is tightly regulated by posttranslational modifications such as phosphorylation, acetylation, sumoylation, neddylation, methylation, glycosylation, and ubiquitination (Brooks and Gu, 2003; Meek and Anderson, 2009). In resting cells, the ubiquitination of p53 by E3 ubiquitin ligases maintains p53 protein at low levels. In contrast, when a cell is exposed to genotoxic stress, p53 is phosphorylated at serine 15 (Ser18 in mouse) by activated ataxia telangiectasia mutated (ATM), a Ser/Thr protein kinase belonging to the PIKK (PI3K [phosphoinositide 3-kinase]-related protein kinase) family (Banin et al., 1998; Canman et al., 1998; Khanna et al., 1998). If the damage to the cell's DNA cannot be repaired, ATM-mediated phosphorylation stabilizes the p53 protein such that it induces the apoptosis of the damaged cell.

A HECT-containing E3 ubiquitin ligase called Mcl-1 ubiquitin ligase E3 (Mule; also known as Huwe1, ARF-BP-1, and Lasu1) has been reported to mediate the polyubiquitination and degradation of p53 (Chen et al., 2005), among other substrates (Adhikary et al., 2005; Liu et al., 2005b; Zhong et al., 2005; Hall et al., 2007; Herold et al., 2008; Zhao et al., 2008; Parsons et al., 2009; Yin et al., 2010). The X-linked *Mule* gene encodes a ubiquitously expressed 4,374-aa protein that contains multiple domains, including BH3. Mule is highly

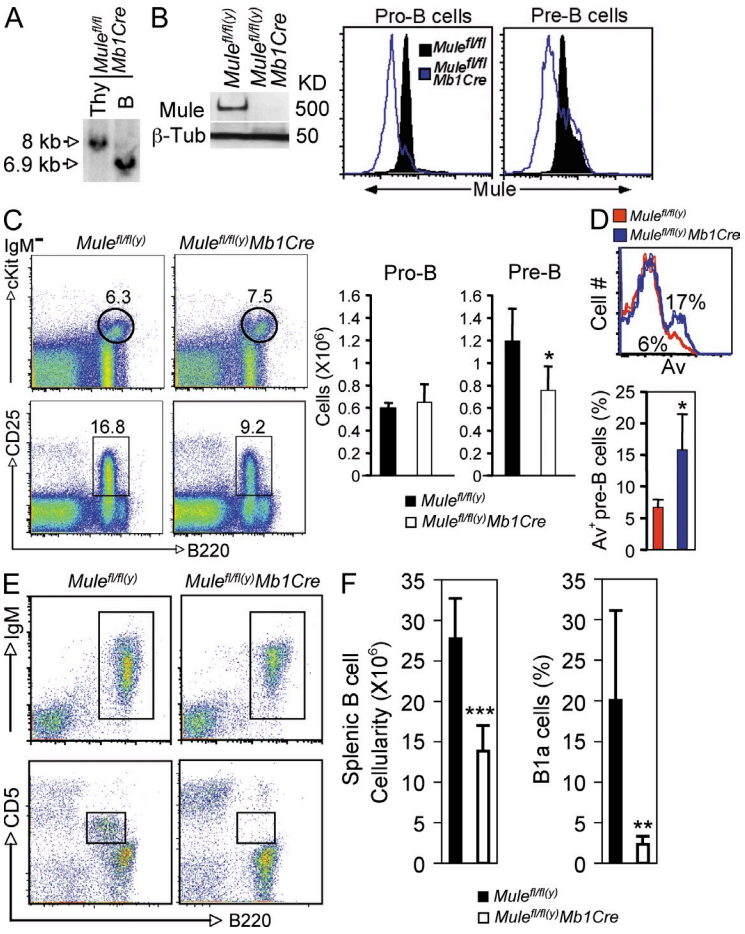

Figure 2. Blockade of B cell development and impaired homeostasis in BMKO mice. (A) Southern blot of lysates of thymocytes (Thy) and splenic B cells from *Mule*$^{fl/fl(y)}$*Mb1Cre* (BMKO) mice. The floxed (8 kb) and deleted (6.9 kb) *Mule* alleles are indicated. (B, left) Immunoblot of purified splenic B cells from control (*Mule*$^{fl/fl(y)}$) and BMKO mice detecting Mule protein. β-Tub, loading control. (B, right) Mule expression in control and BMKO pro– and pre–B cells as determined by flow cytometry. (C, left) Flow cytometric analysis of BM from littermate control and BMKO mice showing the pro–B cell (B220^{low}IgM$^-$cKit$^+$; top) and pre–B cell (B220^{low}IgM$^-$CD25$^+$; bottom) compartments. Numbers are the percentage of the gated IgM$^-$ population. (C, right) Absolute numbers of pro–B cells and pre–B cells in BM isolated from both hind leg femurs (mean ± SD; *, P = 0.006). (D, top) Percentage of apoptotic pre–B cells as determined by flow cytometric analysis of Annexin V expression. (D, bottom) Apoptotic pre–B cells (mean ± SD; *, P = 0.01). Data are from a single experiment involving four to five mice per genotype. (E and F) Flow cytometric analysis of B cell populations in littermate control and BMKO mice. (E, top) Percentage of B220$^+$IgM$^+$ B cells among gated lymphocytes in spleen. (E, bottom) Percentage of CD5$^+$B220$^+$ B1a cells among gated lymphocytes in the peritoneal cavity. Numbers are the percentage among total lymphocytes. (F, left) Splenic B cell cellularity (mean ± SD; ***, P = 1.12^{-5}). (F, right) Percentage of B1a cells in peritoneum (mean ± SD; **, P = 0.0019). Results are representative of two to three (A–C) and three to four (E and F) independent experiments involving one to four mice per genotype.

conserved such that the human and mouse forms share >90% amino acid identity. From a functional viewpoint, the fact that Mule ubiquitinates p53 and other apoptotic molecules suggests that Mule may contribute to the maintenance of cellular homeostasis by preventing inappropriate cell death. In this study, we examined the consequences of Mule deficiency in mouse B cells and mouse embryonic fibroblasts (MEFs). Our analyses reveal a novel mechanism by which Mule acts through the ATM–p53 axis to regulate cellular homeostasis under both steady-state and genotoxic stress conditions.

RESULTS

Generation of conditional *Mule* KO mice

We generated a conditional *Mule* allele (*Mule*^{fl}) in which exons 76 and 77 (encoding the HECT domain) were flanked by *loxP* sites (Fig. 1). *Mule*$^{fl/y}$ male mice were created using Flpe-deleter mice (Rodríguez et al., 2000) and bred with *DeleterCre* females (Schwenk et al., 1995) to produce *Mule*$^{del/+}$ females. According to Mendelian principles, 50% of the male progeny from a cross between a WT male and a *Mule*$^{del/+}$ female should be *Mule*$^{del/y}$ (Mule KO) mice. However, only *Mule*$^{+/y}$ males were born alive, implying that *Mule*$^{del/y}$ mice die before birth (unpublished data). Analysis of *Mule*$^{del/y}$ embryos at embryonic day 9.5 (E9.5) and 10.5 revealed various developmental anomalies, including enlarged heart, reduced somites, and greatly decreased body size compared with controls (unpublished data). The mutant embryos were dead by E12.5, indicating that Mule is essential for mouse embryogenesis.

Loss of Mule impairs B cell development and homeostasis

We chose to characterize the effects of *Mule* deletion in B lymphocytes in adult mice because these cells are known to accumulate p53 and succumb to apoptosis under conditions of genotoxic stress (Murray-Zmijewski et al., 2008). *Mule*$^{fl/y}$ (male) and *Mule*$^{fl/fl}$ (female) mice showed normal B lymphocyte development and subset distribution as determined by flow cytometry (unpublished data). To generate mutants in which *Mule* was selectively deleted in B cells (B cell–specific *Mule* KO [BMKO] mice), *Mule*$^{fl/fl(y)}$ mice (male or female) were crossed to *Mb1Cre* mice in which Cre recombinase is controlled by the B cell–specific *Mb1* promoter (Hobeika et al., 2006). Southern blotting of DNA from purified splenic B cells of BMKO mice confirmed efficient Cre-mediated disruption of *Mule* in B cells but not in thymocytes (Fig. 2 A). Immunoblotting demonstrated the absence of Mule protein in purified splenic BMKO B cells (Fig. 2 B, left). Flow cytometric analysis revealed that *Mule* was also deleted in a large fraction of BMKO pro–B cells and pre–B cells (Fig. 2 B, right).

The main stages of B cell development in the BM are: pro–B (B220^{low}IgM$^-$cKit$^+$), pre–B (B220^{low}IgM$^-$CD25$^+$), immature B (B220^{low}IgM$^+$), and recirculating mature B (B220^{high}IgM$^+$). Although the pro–B cell compartment of BMKO BM was normal,

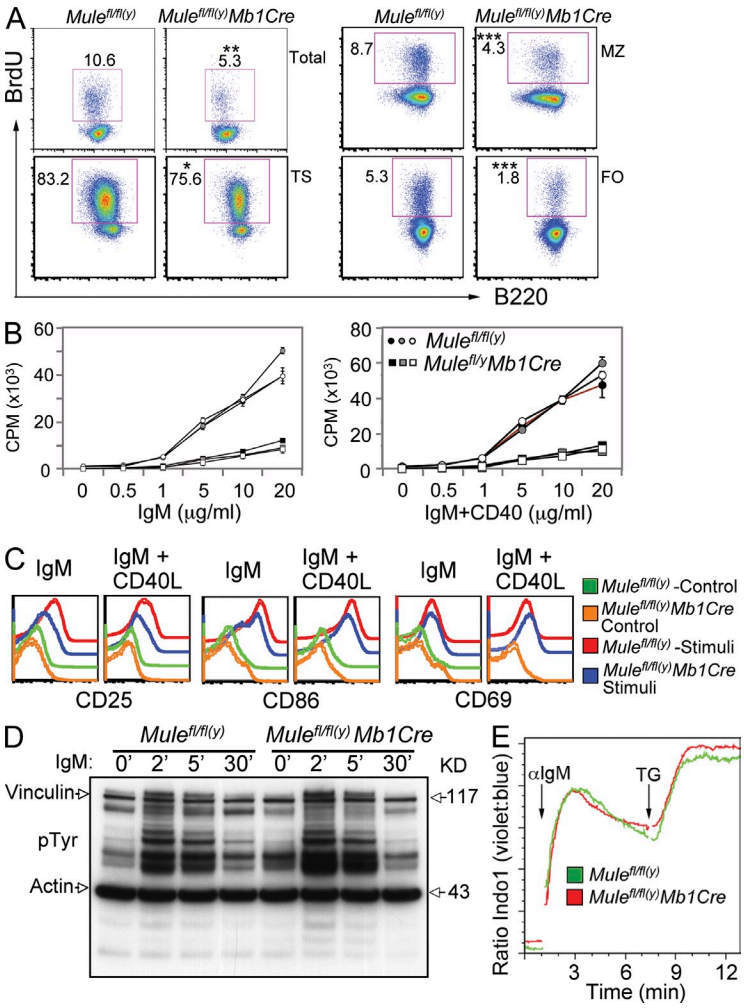

Figure 3. Impaired proliferation and activation of BMKO B cells. (A) Littermate control and BMKO mice were supplied with BrdU-containing drinking water for 3.5 d. Top left, total splenic B cells were stained with anti-BrdU and anti-B220 Abs and analyzed by flow cytometry ($n = 5$; **, $P = 0.0021$). Bottom left, gated $B220^+IgM^+$ cells were further gated on $CD93^+$ and sorted to detect $BrdU^+$ TS B cells ($n = 4$; *, $P = 0.024$). Top right, $B220^+IgM^+$ cells were gated on $CD21^+CD23^{low}$ and sorted to detect $BrdU^+$ MZ B cells ($n = 4$; ***, $P = 0.000077$). Bottom right, $B220^+IgM^+$ cells were gated on $CD21^+CD23^+$ and sorted for $BrdU^+$ FO B cells ($n = 4$; ***, $P = 0.0001$). Numbers are the percentage of $BrdU^+$ cells among the gated population. (B) Purified splenic littermate control and BMKO B cells were stimulated for 24 h with the indicated doses of anti-IgM (left) or anti-IgM plus anti-CD40 (right) and incubated with [^{3}H]-thymidine. Results are the mean ± SD of triplicate. (C) Purified splenic littermate control and BMKO B cells were stimulated with 10 μg/ml anti-IgM or 10 μg/ml anti-IgM plus 0.5 μg/ml CD40 ligand for 24 h. Up-regulation of the indicated activation markers was monitored by flow cytometry. (D) Purified splenic littermate control and BMKO B cells were stimulated with 20 μg/ml anti-IgM for the indicated times. Lysates were immunoblotted to detect phospho-tyrosine (pTyr). (E) Splenic littermate control and BMKO B cells preloaded with Indo-1 were stimulated first with anti-IgM and then with thapsigargin (TG; positive control). The Ca^{2+} response was measured based on the ratio of violet (Ca^{2+} bound) to blue (Ca^{2+} free) fluorescence. Results (A–E) are representative of two to three independent experiments involving one to five mice per genotype.

the pre–B cell compartment in the mutant was significantly decreased compared with controls (Fig. 2 C). Indeed, the pre–B cell population in BMKO mice contained significantly more apoptotic (Annexin V^+) cells than the control (Fig. 2 D). Recirculating $B220^{high}IgM^+$ mature B cells were also reduced by threefold in the mutant BM compared with controls, and apoptotic cells were increased by 1.5-fold (unpublished data). Thus, B cell development is partially blocked in the absence of Mule, and pre–B and mature B cells in BMKO BM are severely reduced as a result of increased apoptosis. When splenic B cells were examined, the percentage of $B220^+IgM^+$ B cells was reduced from 52.3% in controls to 38.5% in the mutant (Fig. 2 E, top). BMKO spleen contained ∼50% fewer cells than control spleen (Fig. 2 F, left). In addition, the B1a cell population that is normally present in the peritoneal cavity of control mice was virtually absent in BMKO mice (Fig. 2, E, [bottom] and F [right]). Thus, Mule is required for B cell development in the BM, as well as the homeostasis of mature B cells in the spleen and B1a cells in the peritoneum.

Impaired proliferation and activation of Mule-deficient B cells

To determine whether impaired proliferation contributed to the reduced B cell numbers in BMKO mice, we performed in vivo BrdU incorporation experiments and observed that the percentage of $BrdU^+$ B cells among total splenic B cells of BMKO mice was only ∼50% of controls (Fig. 3 A, top left). To analyze BrdU incorporation in various B cell subsets, $B220^+IgM^+$ cells from control and BMKO splenocytes were gated and then sorted by flow cytometry into $CD93^+$ transitional (TS), $CD21^+CD23^{low}$ marginal zone (MZ), and $CD21^+CD23^+$ follicular (FO) B cells. The majority of TS B cells were $BrdU^+$ in both control and BMKO mice but the mutant showed significantly fewer of these cells (Fig. 3 A, bottom left). A more striking deficit was found in the mutant MZ compartment, where the percentage of $BrdU^+$ cells was reduced to ∼50% of that in controls (Fig. 3 A, top right). Mule-deficient FO B cells exhibited the most severe defect in proliferation, with the number of $BrdU^+$ cells reaching only ∼30% of the control value (Fig. 3 A, bottom right). [^{3}H]-thymidine incorporation assays confirmed that BMKO B cells proliferated much less vigorously than control B cells in response to stimulation with anti-IgM or anti-IgM plus anti-CD40 (Fig. 3 B). Although the activation marker CD69 was up-regulated normally on stimulated BMKO B cells, levels of CD25 and CD86 up-regulation were decreased compared with controls (Fig. 3 C). Thus, Mule is required for splenic B cell proliferation and activation.

The impaired B cell development in BMKO mice and defective proliferation of BMKO B cells in response to anti-IgM treatment suggested that Mule might be involved in BCR-induced signal transduction, which is initiated by protein

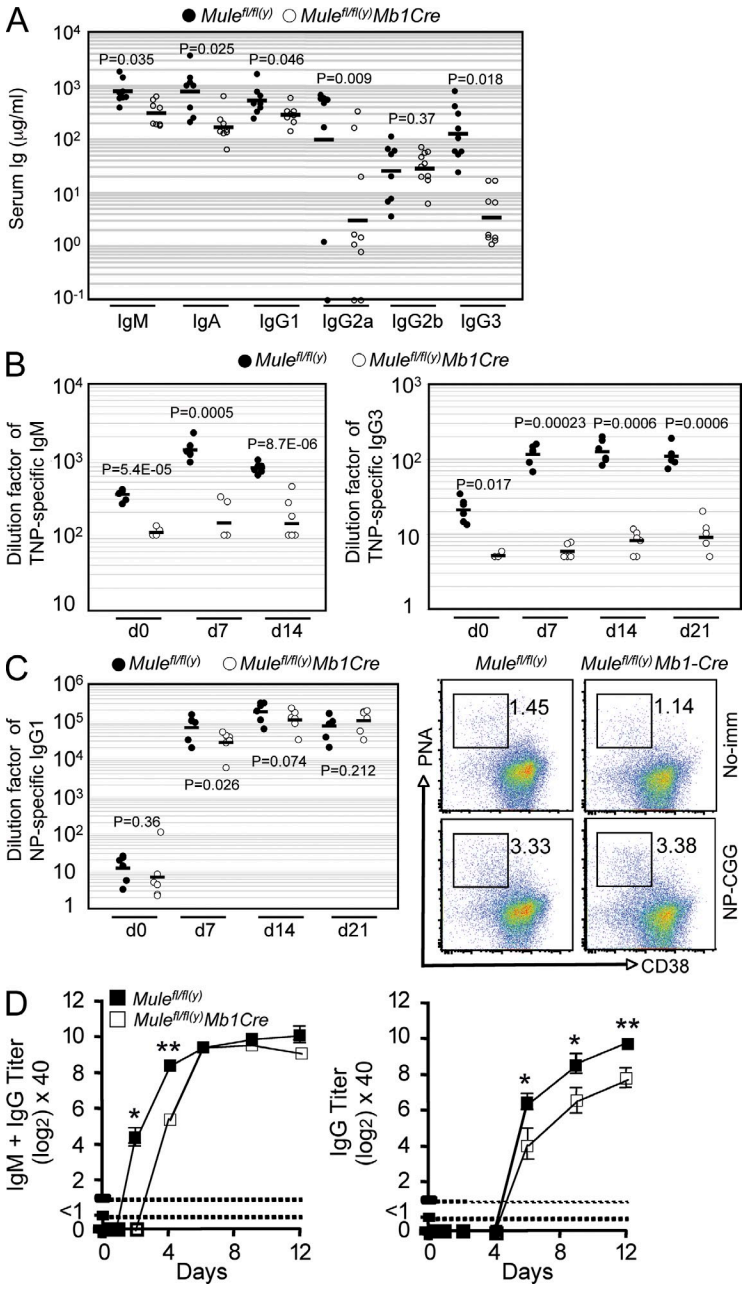

Figure 4. Impaired humoral responses in BMKO mice. (A) Serum from control and BMKO mice (n = 7–10) was analyzed by ELISA to determine levels of the indicated Igs. Horizontal bars are the geometric mean. (B) Littermate control and BMKO mice (n = 6) were i.p. immunized with TNP-Ficoll and serum was analyzed as for A on the indicated days after immunization to detect anti-TNP IgM (left) and anti-TNP IgG3 (right). Results are expressed as a serum dilution factor. Horizontal bars are the geometric mean. (C) Littermate control and BMKO mice (n = 6) were i.p. immunized with $NP_{(15)}$-CGG. Left, serum was analyzed as in B to detect NP-specific IgG1. Right, representative flow cytometric analysis of GC B cells (PNA^{hi}CD38^{lo}) among gated B220^{+} cells from control and BMKO mice before immunization (No-imm) and at 14 d after immunization (NP-CGG). Numbers indicate the percentage of GC B cells. Data shown are from a single experiment involving four to five mice per genotype. Horizontal bars are the geometric mean. (D) Littermate control and BMKO mice (n = 5–6) were i.v. injected with 10^5 pfu VSV. Serum was analyzed on day 0 (before infection) and on days 2, 4, 6, 10, and 12 after VSV infection to detect the total anti-VSV IgM plus IgG titer (left) or the VSV-specific IgG titer (right). Results are the combined mean ± SD (n = 5–6; *, $P < 0.05$; **, $P < 0.005$). Ab titration data are from a single experiment involving 6–10 mice per genotype (A and B), or from two independent experiments involving two to three mice per genotype analyzed together (D).

tyrosine kinases (Kurosaki and Hikida, 2009). However, BCR ligation in purified splenic BMKO B cells resulted in a normal tyrosine phosphorylation pattern (Fig. 3 D). Thus, Mule is unlikely to be involved in BCR-mediated proximal signaling. Consistent with this finding, Ca^{2+} flux in BMKO B cells treated with anti-IgM was also normal (Fig. 3 E). Further investigation is required to dissect how Mule is involved in BCR-induced proliferation and activation.

Mule deficiency severely reduces serum immunoglobulins and humoral immune responses

The involvement of Mule in B cell proliferation and activation prompted us to investigate serum Ig production and humoral immune responses in our BMKO mice. Apart from IgG2b, serum levels of IgM, IgG1, IgA, IgG2a, and IgG3 were reduced by 2.5-, 2-, 4.5-, 32-, and 37-fold, respectively, in nonimmunized BMKO mice compared with controls (Fig. 4 A). However, plasma cell numbers in the BM of mutants and controls were similar (unpublished data), indicating that Mule is involved in Ig production rather than plasma cell differentiation or maintenance.

To determine whether Mule-deficient B cells could mount normal humoral responses, we immunized control and BMKO mice with either the T-independent (Ti) antigen TNP-Ficoll or the T-dependent (Td) antigen alum-precipitated 4-hydroxy-3-nitrophenylacetyl–chicken γ-globulin ($NP_{(15)}$-CGG). When serum was analyzed at 2–3 wk after immunization, Ti-immunized BMKO mice failed to mount a TNP-specific IgM or IgG3 response, whereas Ti-immunized control mice showed normal IgM and IgG3 responses (Fig. 4 B). In contrast, although Td-immunized BMKO B cells produced significantly less NP-specific IgG1 compared with controls at 7 d after immunization, this antibody (Ab) titer was normal at 14 and 21 d after immunization (Fig. 4 C, left). Consistent with this finding, the frequency of GC B cells in BMKO spleens was comparable to controls at day 14 after Td immunization as determined by flow cytometry (Fig. 4 C, right).

To examine the role of Mule in humoral responses in a more physiological setting, we infected BMKO and control mice with vesicular stomatitis virus (VSV). WT mice infected with VSV mount strong humoral responses characterized by

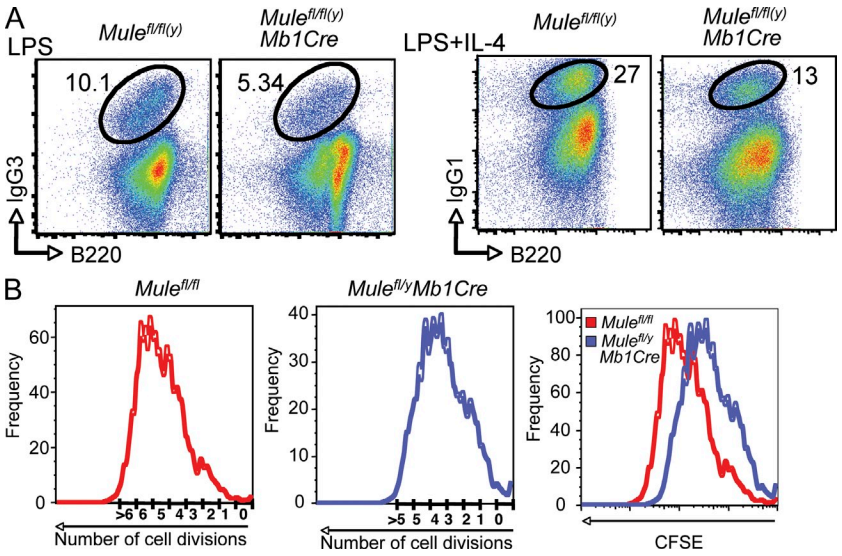

Figure 5. Impaired Ig CSR in Mule-deficient B cells. (A) Purified splenic B cells from mice of the indicated genotypes were stimulated with either LPS (left) or LPS plus IL-4 (right) for 3–5 d and analyzed by flow cytometry to detect IgG3$^+$ class-switched B cells (left) and IgG1$^+$ class-switched B cells (right). Numbers are the percentage of class-switched B cells among gated B cells. Results are representative of three independent experiments involving two to five mice per genotype. (B) Purified splenic B cells were labeled with CFSE and stimulated for 4 d with LPS plus IL-4. Cell divisions tracked by CFSE were analyzed by flow cytometry, with each peak indicating one cell division. Results depicted are representative cell division profiles of littermate control B cells (left), BMKO B cells (middle), and the overlay of control cells over BMKO cells (right). Results from A and B are representative of two independent experiments involving two to three mice per genotype.

a Ti-neutralizing IgM response by days 2–4, followed by a Td IgG response by days 4–6 (Hangartner et al., 2006). In control mice, total VSV-neutralizing Abs (IgM + IgG) appeared by day 2 after infection, peaked on day 4, and remained high until day 12 (Fig. 4 D, left). In contrast, total anti-VSV Abs in BMKO mice were undetectable on day 2 and were only 1/8 of control titers on day 4 after infection. However, by day 6, levels of total anti-VSV Abs in the mutant had caught up to the control, indicating that Mule-deficient B cells can mount an IgM response but with delayed kinetics. When we specifically examined VSV-neutralizing IgG, control mice first exhibited these Abs on day 6 after infection, and their levels continually increased until day 12 after infection (Fig. 4 D, right). However, in BMKO mice, anti-VSV IgG levels were only 1/5 of those in the control on day 6 after infection and failed to achieve control levels even by day 12.

In vitro, B cells undergo class switch recombination (CSR) and differentiate into either IgG3$^+$ plasmablasts in response to LPS or into IgG1$^+$ plasmablasts in response to LPS plus IL-4 (Stavnezer et al., 2008). To determine whether Mule affects CSR, we cultured naive BMKO and control B cells with LPS, or LPS plus IL-4, and measured the percentages of B cells producing IgG3 or IgG1. In both cases, Mule-deficient B cells produced 50% less of the expected isotype than controls (Fig. 5 A). CSR requires that a minimum of two rounds of B cell division be completed to allow IgG production (Hodgkin et al., 1996). To assess whether the CSR defect in BMKO B cells was associated with impaired proliferation, we labeled BMKO and control B cells with CFSE, activated them with LPS plus IL-4, and followed their cell division by flow cytometry. Compared with control B cells, BMKO B cells underwent one cell division less (Fig. 5 B). Thus, Mule is required for proper B cell proliferation and CSR in vitro, as well as normal Ti and Td humoral responses in vivo.

Mule maintains cellular homeostasis under steady-state conditions by controlling p53 activity

We next examined the effect of *Mule* deletion on the function of p53, a known Mule substrate and a key proapoptotic molecule involved in maintaining homeostasis (Chen et al., 2005; Murray-Zmijewski et al., 2008). To aid in these analyses and examine additional cell types, we created Mule-deficient embryonic stem (ES) cell lines and E1A/Ras-transformed Mule-deficient MEFs via Cre-mediated deletion of *Mule*$^{fl/y}$ (Peitz et al., 2002). Immunoblotting showed that, compared with controls, p53 protein was clearly elevated in both Mule-deficient ES cells and MEFs at steady state (Fig. 6 A). Although p53 protein was not detectable by immunoblotting in either BMKO or control B cells at steady state (Fig. 6 A), quantitative real-time PCR analysis showed that mRNA levels of its proapoptotic target genes *Bax*, *Mdm-2*, *Noxa*, *p21*, and *Puma* (Villunger et al., 2003; Green and Kroemer, 2009), including *p53*, were all significantly higher in resting Mule-deficient B cells than in control B cells (Fig. 6 B). These data are consistent with our earlier observation of increased apoptosis in B cells isolated from unstressed BMKO mice (Fig. 2 D). Thus, loss of Mule has profound effects on p53 transcriptional activity at steady state.

To assess whether the increased p53 transactivation in BMKO B cells accounted for their defects, we crossed our BMKO mice to floxed *p53* (*p53*$^{fl/fl}$) mice (Jonkers et al., 2001) to generate compound mutants lacking both Mule and p53 specifically in B cells (B cell–specific double KO [BDKO] mice). Quantitative real-time PCR analysis showed that the abnormal elevations of *Bax*, *Mdm-2*, *Noxa*, and *Puma* mRNAs (but not *p21* mRNA) in BMKO B cells were abrogated upon genetic ablation of p53 (Fig. 6 B). These results suggest that the increase in *Bax*, *Mdm-2*, *Noxa*, and *Puma* mRNAs in BMKO B cells is p53 dependent.

Flow cytometric analysis showed that both the block in BM B cell development at the pre–B cell stage and the defect

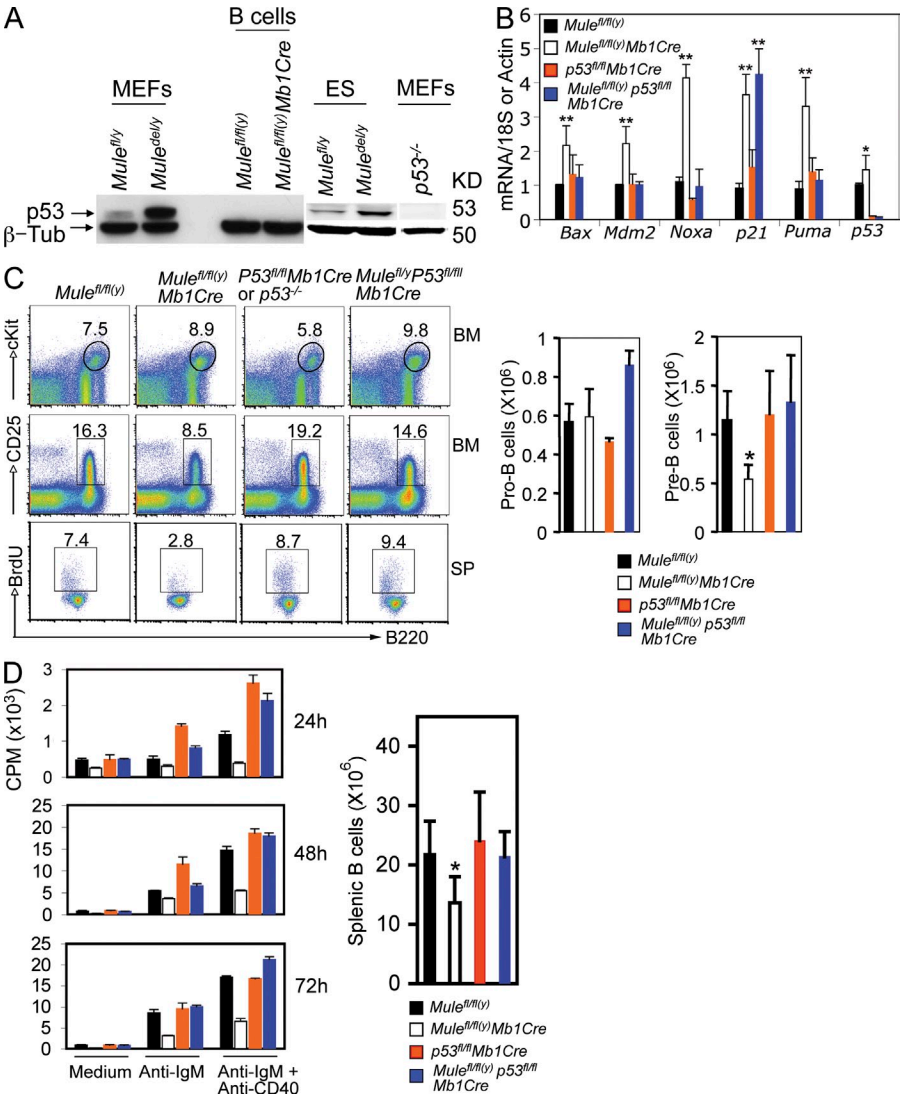

Figure 6. Restoration of B cell homeostasis in BMKO mice by genetic ablation of p53. (A) Lysates of untreated *Mule*$^{fl/y}$ (control) and *Mule*$^{del/y}$ (Mule-deficient) MEFs; control and BMKO B cells; and *Mule*$^{fl/y}$ (control E14K) and *Mule*$^{del/y}$ (Mule deficient) ES cells were immunoblotted to detect total p53 protein. p53$^{-/-}$ MEFs, Ab specificity control. β-Tub, β-tubulin (loading control). MEF and B cell results are representative of two to three independent experiments. ES cell data are from a single experiment involving one control and three Mule-deficient clones. (B) The mRNA expression of the indicated p53 target genes was determined by quantitative real-time PCR in lysates of purified splenic B cells from mice of the indicated genotypes. The relative change in gene expression was calculated using the comparative threshold cycle method ($2\Delta\Delta^{Ct}$). Results are the mean ± SD after normalization to 18S or actin mRNA and are representative of two to five independent experiments involving one to five mice per genotype. P-values (*, $P < 0.05$; **, $P < 0.005$) are from the Student's *t* test of control versus BMKO or BDKO. (C, left) The development of pro–B cells (B220$^+$IgM$^-$cKit$^+$; top row) and pre–B cells (B220$^+$IgM$^-$CD25$^+$; middle row) in the BM of mice of the indicated genotypes was monitored by flow cytometry. The bottom row shows BrdU uptake by total splenic B cells as determined by flow cytometry. Numbers are the percentage of gated IgM$^-$ lymphocytes (top and middle), or of gated B220$^+$ cells (bottom). (C, right) Absolute numbers of pro–B and pre–B cell cells in the BM of mice of the indicated genotypes were determined as in Fig. 2 C. Results are the mean ± SD (*, $P = 0.018$, Student's *t* test of control versus BMKO) and are representative of two to three independent experiments involving one to two mice per genotype. (D, left) purified splenic B cells from mice of the indicated genotypes were treated with 20 μg/ml anti-IgM or 20 μg/ml anti-IgM plus 1 μg/ml anti-CD40 and [^{3}H]-thymidine incorporation was measured at 24, 48, and 72 h after stimulation. Results are the mean± SD and are representative of two independent experiments involving one to two mice per genotype. (D, right) Splenic cellularity of mice of the indicated genotypes was determined as in Fig. 2 F. Results are the combined mean ± SD (*, $P = 0.0073$, Student's *t* test of control versus BMKO) of four independent experiments each involving one to three mice per genotype.

in splenic B cell proliferation disappeared upon genetic ablation of p53 (Fig. 6 C). B cell proliferation in response to anti-IgM or anti-IgM plus anti-CD40 was also restored upon loss of p53 (Fig. 6 D, left), and total B cell numbers in BDKO spleens returned to normal levels (Fig. 6 D, right). Our studies therefore suggest that Mule controls p53 activity essential for B cell development, proliferation, and homeostasis under steady-state conditions.

We noted that our BDKO mice still showed significantly lower levels of serum IgM and IgG1 compared with control mice and B cell–specific p53 KO mice (Fig. 7 A). Consistent with the reduced serum IgG1 in BDKO mice, the impaired LPS-plus-IL-4–induced CSR to IgG1 observed in BMKO B cells was not rescued by genetic ablation of p53 (Fig. 7 B). Indeed, the percentage of class-switched IgG1-producing cells was reduced even further in BDKO B cells, suggesting that both Mule and p53 are indispensable for CSR to IgG1. In addition, the B1a cells missing from the peritoneal cavity of BMKO mice were not restored by loss of p53 (Fig. 7 C). Because B1a cells are a major producer of IgM (Herzenberg, 2000), this finding may account for the reduced serum IgM levels in BMKO and BDKO mice (Fig. 4 A and Fig. 7 A). Notably, deletion of p53 alone in B cells affected neither LPS-plus-IL-4–induced CSR nor B1a cell numbers (Fig. 7, A–C). Thus, the defective CSR, impaired serum Ig production, and lack of B1a cells in BMKO mice are not attributable to increased p53 transactivation.

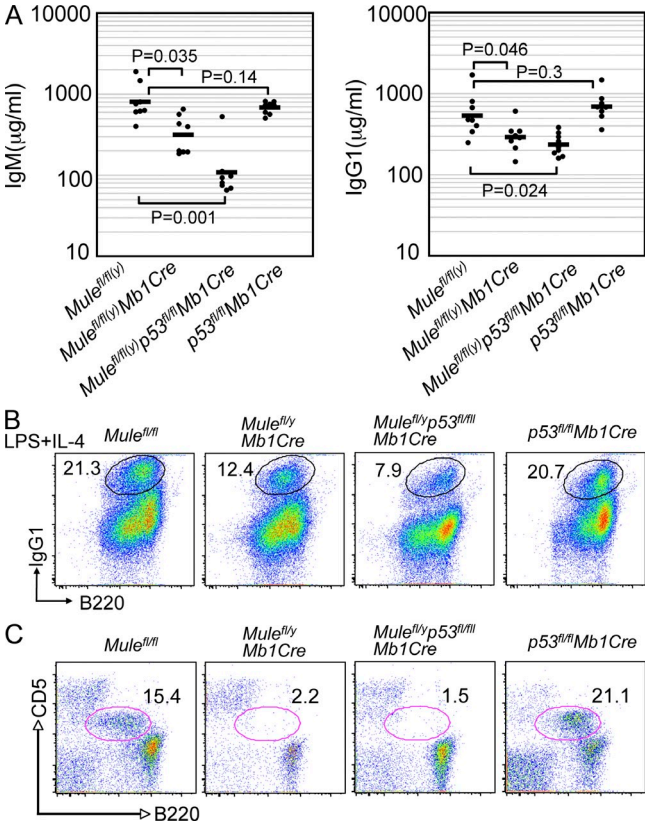

Figure 7. Failure of genetic ablation of p53 in BMKO mice to restore serum Ig levels, Ig class-switching, and B1a cells. (A) Serum IgM (left) and IgG1 (right) levels in unimmunized mice of the indicated genotypes were determined by ELISA. Horizontal bars are the geometric mean. Results shown are from a single experiment involving 6–10 mice per genotype. (B) Purified splenic B cells from mice of the indicated genotypes were stimulated with LPS plus IL-4 for 4 d and the percentage of IgG1$^+$ class-switched B cells was determined by flow cytometry. Numbers indicate the percentage of class-switched B cells among gated B cells. (C) The percentage of B1a cells (CD5$^+$B220$^+$) in the peritoneal cavity of mice of the indicated genotypes was determined by flow cytometry. For B and C, results are representative of two to three independent experiments involving one to three mice per genotype.

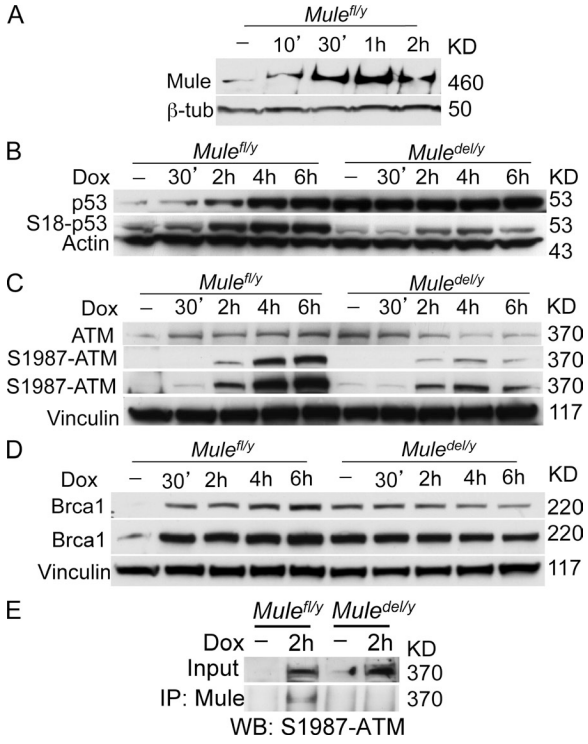

Figure 8. Abnormal ATM–p53 axis function in Mule-deficient MEFs. (A) *Mule*$^{fl/y}$ MEFs were treated with 1 μM Dox for the indicated times and extracts were immunoblotted to detect Mule. (B) *Mule*$^{fl/y}$ and *Mule*$^{del/y}$ MEFs were left untreated (−) or treated with 1 μM Dox for the indicated times. Total p53 and phospho-p53-Ser18 (S18-p53) were detected by immunoblotting. (C) *Mule*$^{fl/y}$ and *Mule*$^{del/y}$ MEFs were treated as in B, and total ATM and phospho-ATM-Ser1987 were detected by immunoblotting. For phospho-ATM, film exposures of 30 s (row 2) and 5 min (row 3) are shown. Vinculin, loading control. (D) *Mule*$^{fl/y}$ and *Mule*$^{del/y}$ MEFs were treated as in C and total Brca1 was detected by immunoblotting. Film exposures of 2 s (row 1) and 30 s (row 2) are shown. (E) *Mule*$^{fl/y}$ and *Mule*$^{del/y}$ MEFs were left untreated (−) or treated for 2 h with 1 μM Dox. Lysates were immunoprecipitated with anti-Mule Ab followed by immunoblotting (WB) with anti–phospho-ATM-Ser1987 Ab. Input, total cell lysate subjected to immunoprecipitation with anti-Mule Ab. For A–E, data are representative of two independent experiments.

Mule maintains homeostasis under genotoxic stress conditions through the ATM–p53 axis

To examine how Mule regulates p53 protein levels under stress conditions, we treated Mule-deficient MEFs and BMKO B cells with genotoxic agents known to elicit a p53-dependent response. Control MEFs treated with doxorubicin (Dox) exhibited up-regulation of Mule protein as early as 10 min after Dox treatment (Fig. 8 A). p53 protein gradually accumulated in Dox-treated control MEFs and became phosphorylated at Ser18 (Fig. 8 B, left). Consistent with p53 being a Mule substrate (Chen et al., 2005), high levels of p53 protein were present in Mule-deficient MEFs even at steady state (Fig. 8 B, right, top row). However, phosphorylation of this p53 in response to Dox treatment was impaired (Fig. 8 B, right, middle row). Because genotoxic stress induces p53 phosphorylation by activated ATM (Lavin, 2008), we next examined ATM phosphorylation in the absence of Mule. In Dox-treated control MEFs, total ATM protein accumulated with time (Fig. 8 C, top row) and became phosphorylated at Ser1987 by 2 h after stimulation (Fig. 8 C, middle row). However, consistent with their decreased phospho-p53, Dox-treated Mule-deficient MEFs showed much lower levels of phospho-ATM (Fig. 8 C). Another relevant substrate of phospho-ATM is Brca1 (Cortez et al., 1999). In response to Dox treatment, Brca1 accumulated in a time-dependent manner in control MEFs but not in Mule-deficient MEFs (Fig. 8 D). Intriguingly, low levels of phospho-ATM and high levels of Brca1 were present in Mule-deficient MEFs even without genotoxic stress (Fig. 8, C and D), whereas control MEFs showed no detectable phospho-ATM or Brca1 at steady state. To investigate whether there was a physical interaction between Mule and ATM that might account for our

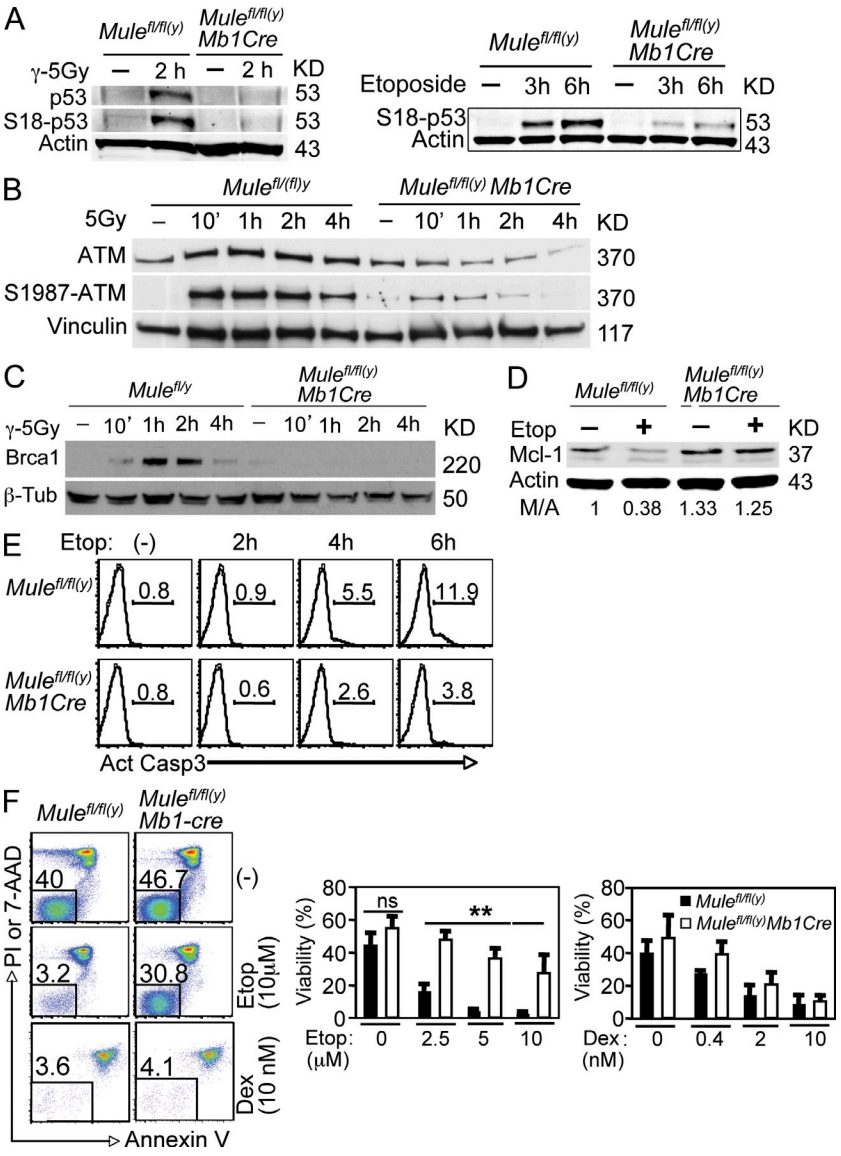

Figure 9. Abnormal ATM–p53 axis function in Mule-deficient B cells. (A) Purified splenic control and BMKO B cells were treated with γ-irradiation (5Gy) for 2 h (left), or 10 μM etoposide for 3 or 6 h (right), followed by immunoblotting to detect phospho-p53-Ser18 (S18-p53). (B) Purified splenic littermate control and BMKO B cells were γ-irradiated (5 Gy) followed by immunoblotting to detect phospho-ATM-Ser1987 (S1987-ATM) at the indicated times after irradiation. (C) Purified splenic control and BMKO B cells were treated as in B. Total Brca1 was detected by immunoblotting. (D) Purified splenic control and BMKO B cells were treated with 10 μM etoposide (Etop) for 6 h and degradation of Mcl-1 was monitored by immunoblotting. M/A is the ratio of Mcl-1 protein to actin protein as determined by densitometry (the ratio in unstimulated controls was defined as 1). (E) Purified splenic littermate control and BMKO B cells were treated with 10 μM etoposide for 2, 4, or 6 h followed by detection of cleaved (activated) caspase-3 by flow cytometry. Numbers are the percentage of B cells positive for cleaved caspase-3. Results are representative of a single experiment involving three mice per genotype. (F) Purified splenic littermate control and BMKO B cells were treated with the indicated doses of etoposide or dexamethasone (Dex) for 20–24 h and viability was determined by flow cytometric analysis of Annexin V versus propidium iodide or 7AAD (7-amino-actinomycin D) expression. Left, representative flow cytometry plot. Numbers are percentages of viable cells. Right, quantitation of viability. Results are the combined mean ± SD of three to five independent experiments each involving one to three mice per genotype (**, $P < 0.005$; ns, not significant). For A–D, results are representative of two to three independent experiments.

observations, protein lysates from control MEFs that were left untreated or treated with Dox for 2 h were subjected to immunoprecipitation with anti-Mule Ab followed by anti–phospho-ATM (S1987) immunoblotting. The results showed that Mule was able to interact with phospho-ATM (Ser1987) after Dox treatment (Fig. 8 E, left). The specificity of this interaction was confirmed in a parallel immunoprecipitation experiment using Mule-deficient MEFs (Fig. 8 E, right).

As we are aware that the interpretation of p53-related experiments in E1A transformed MEFs may be equivocal, we extended our investigations in primary B cells. We exposed control and BMKO splenic B cells to two different genotoxic agents. Consistent with our MEF analyses, Mule was up-regulated in control splenic B cells as soon as 10 min after exposure to γ-irradiation (unpublished data). Although our earlier data showed that p53 protein was undetectable in control splenic B cells at steady state (Fig. 6 A), p53 protein was both stabilized and efficiently phosphorylated at Ser18 in control B cells subjected to γ-irradiation for 2 h (Fig. 9 A, left). However, neither stabilization nor Ser18 phosphorylation of p53 (phospho-p53-Ser18) was observed in γ-irradiated BMKO B cells (Fig. 9 A, left). Similarly, control B cells (but not BMKO B cells) treated with etoposide accumulated phospho–p53-Ser18 (Fig. 9 A, right). In γ-irradiated control B cells, total ATM protein accumulated with time and became phosphorylated at Ser1987 by 60 min after stimulation (Fig. 9 B, left). In contrast, consistent with their decreased phospho-p53-Ser18, γ-irradiated BMKO B cells showed much lower levels of both total ATM and phospho-ATM (Fig. 9 B, right). As we had observed for MEFs (Fig. 8 C), spontaneous phosphorylation of ATM at Ser1987 occurred in BMKO B cells (but not in control B cells) even in the absence of genotoxic stress (Fig. 9 B, middle row). Again replicating our observations in stressed MEFs, Brca1 protein readily accumulated in γ-irradiated control B cells but not in BMKO B cells (Fig. 9 C). Thus, Mule is required for efficient phosphorylation of ATM and induction of some of its substrates.

Although Mcl-1 is a known substrate for Mule's E3 ubiquitin ligase activity, only slightly more Mcl-1 protein was present in BMKO B cells than in control B cells at steady state (Fig. 9 D). To investigate whether stress-induced Mcl-1 degradation is mediated by Mule, we treated purified splenic control and BMKO B cells with etoposide and analyzed lysates of these cells by immunoblotting. Mcl-1 protein degradation was highly efficient in stressed control B cells but largely inhibited in stressed BMKO B cells (Fig. 9 D), indicating that the E3 ubiquitin ligase activity of Mule is critical for controlling Mcl-1 protein levels in response to genotoxic stress. Consistent with their impaired Mcl-1 degradation and decreased p53 accumulation and phosphorylation, BMKO B cells treated with etoposide for 4–6 h showed a two to threefold reduction in caspase-3 and -9 cleavage (Fig. 9 E and not depicted) and were consequently resistant to etoposide-induced apoptosis (Fig. 9 F). However, BMKO B cells were just as sensitive as control B cells to apoptosis induced by dexamethasone (Fig. 9 F), which is a p53-independent stimulus. Thus, Mule is required for Mcl-1 degradation and proper ATM-mediated p53 responses to genotoxic stress.

In summary, our results show that, in addition to targeting Mcl-1 and p53 for polyubiquitination and degradation (Chen et al., 2005; Zhong et al., 2005), Mule is required for the regulation of ATM and its substrates. Importantly, this regulation is required to maintain cellular homeostasis under both steady-state and genotoxic stress conditions.

DISCUSSION

Protein ubiquitination plays key roles in the transcriptional regulation and signal transduction that control the balance between cell survival and cell death (Liu et al., 2005a). Mule has been identified as an E3 ubiquitin ligase that polyubiquitinates p53 and targets it for proteasomal degradation (Chen et al., 2005). In this study, we present data from examinations of Mule-deficient B cells and MEFs which indicate that Mule is essential for cellular homeostasis under both resting and stress conditions.

We found that B cell development, proliferation, homeostasis, and immune responses were impaired in BMKO mice, and that Mule maintains B cell homeostasis at steady state by regulating p53 activity. Elevated p53 transactivation is largely responsible for the blockade of B cell development and disturbed B cell functions observed in unstressed BMKO mice, as indicated by the rescue of these phenotypes upon genetic ablation of p53. Given that Mule-deficient B cells expressed a basal low level of phospho–ATM-S1987 that was not observed in control cells, we speculate that this activated ATM may constitutively phosphorylate p53 and activate it sufficiently to at least partially account for the two to fourfold increase in p53 transactivation seen in the mutant cells. In addition to increasing apoptosis, this elevated p53 transactivation could trigger cell cycle arrest. This hypothesis is supported by our observation of decreased BrdU incorporation by BMKO splenic B cells compared with controls. We recognize that further investigation is needed to clarify the extent to which cell cycle arrest contributes to the B cell deficit caused by loss of Mule. However, the abrogation of the abnormal increase in *Puma* and *Noxa* mRNAs in BMKO B cells upon genetic ablation of *p53* argues in favor of the interpretation that p53–mediated apoptosis is responsible for the B cell defects seen in BMKO mice. Genetic ablation of *Puma* in BMKO mice through genetic breeding should resolve this issue clearly. Finally, although BMKO B cells exhibited elevated p53 transactivation, total p53 protein levels remained below the limit of detection by immunoblot. Consequently, we cannot be certain that p53 protein levels were coordinately increased in these cells, although elevated p53 protein was detected in both Mule-deficient MEFs and ES cells under the same conditions. In any case, these data suggest that Mule may influence the transactivation and functions of p53 in a manner that is not exclusively dependent on p53 polyubiquitination and degradation.

Modulation of p53–Mdm2 interaction is essential for normal p53 activity because genetic ablation of p53 prevents the lethality of *Mdm2* KO mice (Brooks and Gu, 2006). B cell–specific *Mdm2* deletion prevents any B cell development in these animals (unpublished data), a more severe phenotype than that resulting from B cell–specific loss of Mule. Because both Mule and Mdm2 target p53 for polyubiquitination and degradation, it is reasonable to speculate that Mule might compensate for the loss of Mdm2 in Mdm2-deficient mice and vice versa. However, the embryonic lethality of both *Mule*-null and *Mdm2*-null mice, and the defective B cell development in B cell–specific *Mule* and B cell–specific *Mdm2* KO mutants, suggest that Mule and Mdm2 have nonoverlapping functions in maintaining p53 levels. Thus, both Mdm2 and Mule are needed to maintain p53 protein at the appropriate low levels at steady state.

Although p53 ablation rescued the defective B cell development, proliferation, and homeostasis in BMKO mice, it failed to restore normal B1a cells, CSR, or serum Ig levels. We speculate that the latter two deficits may be related to the impaired ATM activation in BMKO B cells. ATM-deficient mice show defects in B cell CSR and serum Ig levels that partially mirror those in BMKO mice (Xu et al., 1996; Lumsden et al., 2004). Because ATM stabilizes the DNA double-strand breaks required for Ig gene assembly (Bredemeyer et al., 2006), it is possible that some of the effects of Mule deficiency on B cell development are mediated through ATM. In addition, given that siRNA knockdown of Mule leads to increased DNA repair in manner dependent on DNA polymerase β (Parsons et al., 2009), loss of Mule in B cells could quite conceivably lead to defects in RAG-mediated V(D)J recombination. However, BMKO and control mice showed comparable percentages of intracellular Ig μ^+ cells among $B220^+CD43^+$ BM B cells (unpublished data). Consistent with this finding, the Ig κ-to-λ light chain ratio in newly formed splenic B cells is not altered in BMKO mice. These results suggested that neither RAG-mediated V(D)J recombination of the Ig H locus and its expression nor the λ light chain usage are affected by loss of Mule. Thus, Mule is unlikely to be required for events associated with DNA recombination in B cells.

Given that Mule has multiple substrates, it is not surprising that Mule has different regulatory effects on different cell types. In neurons, Mule controls differentiation and proliferation in vivo by destabilizing its substrate N-Myc (Zhao et al., 2008). In our study, we have shown that Mule regulates B cell development, proliferation, and homeostasis through the ATM–p53 axis. Although Mule was previously identified as an ATM substrate in screening studies, the biological implications of Mule–ATM interaction were not explored (Matsuoka et al., 2007; Mu et al., 2007). Our study has unearthed the intriguing possibility that Mule plays opposite roles in ATM phosphorylation depending on whether the cell is at steady state or has experienced DNA damage. We theorize that, under steady-state conditions, Mule is required to suppress ATM phosphorylation, thereby preventing excessive activation of p53 that could disrupt cellular homeostasis. However, during responses to genotoxic stress, Mule protein quickly accumulates and binds to phospho-ATM. The importance of this Mule–ATM interaction is highlighted by the impaired ATM accumulation and phosphorylation observed in both Mule-deficient B cells and MEFs treated with DNA-damaging agents. Without Mule, neither of the ATM substrates phospho-p53 nor Brca1 can be efficiently induced. Thus, Mule is directly or indirectly involved in the ATM-mediated response to DNA damage. In support of this hypothesis, we have found that the numbers of ATM foci and 53BP1 foci induced by DNA damage are greatly reduced in Mule-deficient MEFs compared with controls (unpublished data). Whether Mule itself participates in the DNA damage response through its interaction with ATM, or whether it is Mule's ubiquitination of its known substrates (such as histones [Liu et al., 2005b], TopBP1 [Herold et al., 2008], and/or DNA polymerase [Parsons et al., 2009]) that is important, remains to be determined.

In conclusion, we have demonstrated crucial functions for Mule in regulating the ATM–p53 axis under both steady-state and genotoxic stress conditions. Disruption of Mule function in various cell types leads to developmental and functional deficits that implicate this E3 ubiquitin ligase as a key player in a new molecular network required for the maintenance of cellular homeostasis.

MATERIALS AND METHODS

Mice. *Mule* floxed ($Mule^{fl/fl(y)}$) mice were generated using Cre/*LoxP* recombination and the gene targeting and screening strategies outlined in Fig. 1. The experimental procedures used for the culture, transfection, and selection of E14K ES cells (129/Ola) have been previously described (Hao and Rajewsky, 2001). Chimeric mice were crossed to Flpe-deleter mice (Rodríguez et al., 2000) to generate $Mule^{fl/fl(y)}$ mice.

To generate BMKO mice (*Mule* deleted specifically in B cells), $Mule^{fl/fl(y)}$ mice were bred with *Mb1Cre* mice (C57BL/6; Hobeika et al., 2006). The resulting $Mule^{fl/fl(y)}Mb1Cre$ mice were backcrossed for 6–10 generations to C57BL/6. p53 was deleted in $Mule^{fl/fl(y)}Mb1Cre$ mice by crossing to $P53^{fl/fl}$ mice (Jonkers et al., 2001). The resulting $Mule^{fl/+(y)}P53^{fl/+}$ F1 mice, with or without *Mb1Cre*, were intercrossed to generate $Mule^{fl/fl(y)}P53^{fl/fl}Mb1Cre$ mice (BDKO mice; mixed genetic background). Because Cre expression can be toxic to cells (Schmidt-Supprian and Rajewsky, 2007), we included $Mule^{fl/+}$ *Mb1Cre*, $P53^{fl/+}Mb1Cre$ and $Mule^{fl/+}P53^{fl/+}Mb1Cre$ mice in all initial analyses of the corresponding mutants. These control mice were phenotypically indistinguishable from the control $Mule^{fl/fl(y)}$ animals used in this study, as judged by cellularity and size of spleen. Mice used in experiments were ≥2 mo old unless otherwise specified. All animal experiments were approved by the University Health Network Animal Care Committee.

Immunoblotting and immunoprecipitation. Cells were lysed in 0.5% NP-40 lysis buffer (20 mM Tris-HCl, pH 8, 137 mM NaCl, 10% glycerol, 0.5% NP-40, and 2.5 mM EDTA), or RIPA buffer (50 mM Tris-HCl, pH 8, 150 mM NaCl, 0.5% NP-40, 0.5% sodium deoxycholate, and 0.1% SDS), with protease inhibitor and phosphatase inhibitor (Roche) freshly added. Lysates were incubated on ice for 30 min and cleared by centrifugation. Protein concentrations in lysates were determined using the BCA protein assay (Thermo Fisher Scientific). Cell lysates (20–100 μg) were loaded onto 4–12% bis-Tris gels to detect proteins below 200 kD, or onto 3–8% Tris-acetate gels to detect Mule. Fractionated proteins were transferred to a nitrocellulose membrane by i-Blot according to the manufacturer's instructions (Invitrogen). The membranes were immunoblotted using Abs recognizing the following: ATM (GeneTex); Ser1987-ATM (Rockland); Brca1 (Santa Cruz Biotechnology, Inc.); p53 (Santa Cruz Biotechnology, Inc.); Ser18-p53 (R&D Systems); and phospho-tyrosine (Millipore). Infrared dye-labeled secondary Abs (anti–rabbit Alexa Fluor 680 [Invitrogen] and anti–mouse IR800 [LI-COR Biosciences]) were visualized with an Odyssey scanner (LI-COR Biosciences).

For immunoprecipitations, cell lysates prepared from 10^8 MEFs were incubated with anti-Mule Ab and protein G–Sepharose beads at 4°C overnight. Immunocomplexes were washed five times with lysis buffer, followed by standard immunoblotting analysis as described in the previous paragraph.

Flow cytometry. Single cell suspensions were prepared from spleen or BM preparations that had been treated to lyse red blood cells. Cells ($1–2 \times 10^6$) were preincubated with Fc block for 15 min at 4°C and immunostained with Abs recognizing the following: IgM (II/41), IgD (11-26c.2a), IgG1 (X56), IgG3 (R40-82), Ig κ light chain (187.1), Ig λ light chain (R26-46), CD5 (53–7.3), CD9 (KMC8), CD16/CD32 (2.4G2), CD21 (7G6), CD23 (B3B4), CD24 (M1/69), CD25 (PC61), CD38 (90), CD43 (S7), CD45R/B220 (RA3-6B2), CD69 (H1.2F3), CD86 (GL1), CD93 (AA4.1), or CD117/cKit (2B8; all obtained from BD or eBioscience unless otherwise specified). A mouse mAb against bacterially expressed Mule (aa 2375–2491) was generated by ProMab and used to detect Mule protein in immunoblotting and intracellular flow cytometry experiments. This anti-Mule mAb recognizes a specific 480-kD band in mouse cell extracts, as confirmed in Mule-deficient MEFs. Fluorescein-labeled PNA (peanut agglutinin) was used to detect GCs (Vector Laboratories). Flow cytometry data were acquired using either a FACSCalibur (BD) or FACSCanto (BD) flow cytometer, and analyzed with either the CellQuest software (BD) or the FlowJo analysis program (Tree Star).

Intracellular staining of Mule was performed as described previously (Hao et al., 2008). In brief, BM cells were fixed with 1.6% paraformaldehyde and incubated for 30 min at RT. After one wash in PBS, ice-cold methanol (100%) was added dropwise and cells were incubated on ice for 30 min. Washed cells were incubated for 30 min with Abs recognizing B220 (RA3-6B2), CD43 (S7), IgM (II/4.1), or Mule. Immunostained cells were incubated with Alexa Fluor 488– or Alexa Fluor 647–conjugated rabbit anti–mouse IgG and analyzed by flow cytometry.

For intracellular Ig μ staining, BM cells were first surface stained with the following fluorescent Abs recognizing B220, IgM, CD43, or CD25. $B220^+IgM^-CD43^+CD25^-$ cells were sorted by flow cytometry, fixed, and permeabilized using the Cytofix/Cytoperm kit according to the manufacturer's instructions (BD). Fixed cells were stained with FITC–anti-IgM (II/4.1) and analyzed by flow cytometry.

For BrdU staining, mice were supplied with BrdU-containing drinking water (1 mg/ml) for 3.5 d. Total splenic B cells were isolated and immunostained as described in the previous paragraph, and sorted into TS ($B220^+IgM^+CD93^+$), MZ ($B220^+IgM^+CD21^+CD23^{low}$), and FO

($B220^+IgM^+CD21^+CD23^+$) subpopulations by flow cytometry. BrdU incorporation in each subset was detected by flow cytometry using the BrdU-Flow kit according to the manufacturer's instructions (BD).

Ca^{2+} flux. Splenocytes were stained using FITC-conjugated anti-B220 Ab as described in the previous section. 1×10^7 stained cells were incubated at 37°C for 45 min with 5 μg/ml Indo-1 AM (Invitrogen) in RPMI-1640 medium supplemented with 10% FCS. Indo-loaded cells were resuspended at 5×10^6/ml and kept on ice until use. 500-μl aliquots of Indo-loaded cells were warmed to 37°C for 10 min and a baseline reading was acquired for 1 min. Ca^{2+} flux induction was triggered by the addition of 20 μg/ml goat anti–mouse IgM (Jackson ImmunoResearch Laboratories, Inc.) followed, 7 min later, by addition of 100 nM thapsigargin as a positive control. Data collection was continued for another 5 min. The Ca^{2+} response was measured based on the ratio of violet (Ca^{2+} bound) to blue (Ca^{2+} free) fluorescence as detected by flow cytometry (LSRII; BD).

[^{3}H]-thymidine incorporation. Purified splenic B cells were seeded in triplicate in 96-well U-bottom plates at 10^5 cells/200 μl in RPMI-1640 containing 10% FCS. Cells were left untreated, or stimulated with various doses of anti-IgM (Jackson ImmunoResearch Laboratories, Inc.), or with anti-IgM plus 1 μg/ml anti-CD40 (BD). At 16, 40, or 64 h after seeding with stimuli, [^{3}H]-thymidine (1 μCi) was added to each well and cells were cultured for another 8 h to determine proliferation at 24, 48, or 72 h [^{3}H]-thymidine uptake was assessed using a liquid scintillation β-counter (TopCount reader).

Humoral immune responses. Mice were immunized i.p. with either 25 μg of the Ti antigen TNP-Ficoll in PBS, or 100 μg of the alum-precipitated Td antigen $NP_{(15)}$-CG (Biosearch Technologies). Assays were performed using 96-well ELISA plates coated with 20 μg/ml TNP-BSA or 10 μg/ml $NP_{(15)}$-BSA. Serum samples collected on day 0 (before immunization) and on days 7, 14, and 21 after immunization were serially diluted and applied to the ELISA plates. Bound Abs were detected by the addition of biotinylated goat anti–mouse IgM, IgG1, and IgG3 (Santa Cruz Biotechnology, Inc.). Biotin binding was revealed using streptavidin-HRP and its substrate. Absorbance at 450 nm was measured using a FlexStation Microplate Reader (Molecular Devices).

VSV infection. VSV infection was performed as previously described (Junt et al., 2002). In brief, mice were i.v. injected with 10^5 pfu VSV-Indiana strain (VSV-IND, Mudd-Summers isolate). Virus was propagated on BHK-21 cells at an MOI of 0.01 and plaqued on Vero cells. During survival experiments, the health status of mice was checked twice daily. Upon appearance of clinical signs of VSV replication in the CNS, such as paralysis or scrubby pelt, mice were removed from the experiment and counted as dead.

For Ig analyses, serum samples collected on days 0, 2, 4, 6, 10, and 12 after infection were diluted 40-fold in MEM containing 2% FCS. For the detection of neutralizing IgM and IgG, various serum dilutions were incubated with 500 pfu VSV-Ind for 90 min followed by transfer to a single cell layer of Vero cells and incubation for 1 h. After addition of an overlay (1:1 MEM/2% methylcellulose), cells were incubated overnight before fixation and staining for 1 h with 0.5% crystal violet (Sigma-Aldrich). The dilution that resulted in a 50% reduction in virus plaques was taken as the neutralizing titer. For IgG titers, serum samples were incubated with an equal volume of 0.1 M β-ME in PBS for 1 h at RT before dilution. Before use in experiments, all mouse sera were heated at 56°C for 30 min to inactivate complement.

CSR. Purified splenic B cells were cultured for 3–5 d in RPMI-1640 containing 10% FCS plus either 20 μg/ml LPS (InVivo Gene) or 20 μg/ml LPS plus 100–200 U/ml IL-4 (PeproTech). The percentages of B cells that had undergone class-switching to production of IgG3 or IgG1 were determined by flow cytometry.

CFSE labeling. Purified splenic B cells were incubated with 1 μM CFSE (Invitrogen) in serum-free RPMI-1640 medium for 10 min at 37°C with gentle mixing. After two washes, the labeled cells were seeded at a density of 5×10^6 cells/ml in RPMI-1640 containing 10% FCS. Labeled cells were stimulated with 20 μg/ml LPS plus 100–200 U/ml IL-4 for 3–5 d. The proliferation capacity of the stimulated B cells was measured by flow cytometry as denoted by a decrease in CFSE fluorescence intensity.

Generation of Mule-deficient MEFs. MEFs derived from E14.5 embryos arising from the crossing of $Mule^{fl/+}$ and $Mule^{fl/y}$ mice were transformed with pLPC-E1A-IRES-Ras^{V12} according to a standard protocol. Transformed $Mule^{fl/y}$ MEFs were transduced with His-TAT-NLS-Cre (Peitz et al., 2002), followed by limiting dilution and expansion to screen for single clones that had undergone Cre-mediated deletion of the floxed *Mule* allele. The elimination of Mule protein in MEFs was confirmed by immunoblotting as described in Immunoblotting and immunoprecipitation.

Generation of the Mule-deficient ES cell line. Targeted ES cell clones were transiently transfected with a Cre-encoding plasmid to delete the distal, loxP-flanked exons 76 and 77 of the mouse *Mule* gene as well as the neomycin resistance gene. DNA samples from neomycin-sensitive clones were digested with StuI and hybridized to probe c, as depicted in Fig. 1. The appearance in these mutants of only a band of 6.9 kb confirmed the total deletion of the targeted *Mule* exons. The elimination of Mule protein in ES cells was confirmed by immunoblotting as described in Immunoblotting and immunoprecipitation.

Real-time PCR. Total RNA was extracted from purified splenic B cells using the RNeasy kit (QIAGEN) according to the manufacturer's protocol. Extracted RNAs were reverse transcribed using random hexamers and the SuperScript III kit (Invitrogen) as per the manufacturer's protocol. The resulting cDNAs were diluted 1:10 and served as templates for real-time PCR reactions using the *Power* SYBR-Green PCR Master Mix (Applied Biosystems). The optimization of the real-time PCR reaction was performed according to the manufacturer's instructions but was scaled down to a 10-μl final reaction volume containing 500 nM forward primer and 500 nM reverse primer. The PCR reaction mixtures were preincubated at 50°C for 2 min, followed by denaturation at 95°C for 10 min, and 40 cycles of 95°C for 15 s and 60°C for 1 min, using the ABI 7700HT Fast Real-Time PCR System (Applied Biosystems). Data were analyzed using SDS software (Applied Biosystems).

Primer sequences were as follows: p21 forward, 5′-GGCCCGGAACATCTCAGG-3′; p21 reverse, 5′-AAATCTGTCAGGCTGGTCTGC-3′; Puma forward, 5′-TCACCCTGGAGGGTCATGTA-3′; Puma reverse, 5′-GCGGGTGTAGGCACCTAGT-3′; Noxa forward, 5′-ATCAAGGGCTGAAGGGATTT-3′; Noxa reverse, 5′-AGAGAGGCACCTGGGATATG-3′; Mdm2 forward, 5′-CCAGCTTCGGAACAAGAGAC-3′; Mdm2 reverse, 5′-GTCGTTTTGCGCTCCAAC-3′; Bax forward, 5′-TGGAGATGAACTGGACAGCA-3′; Bax reverse, 5′-GAAGTTGCCATCAGCAAACA-3′; p53 forward, 5′-ACTGCATGGACGATCTGTTG-3′; and p53 reverse, 5′-GTGACAGGGTCCTGTGCTG-3′. Each sample was assessed in triplicate. Relative mRNA levels were normalized to the housekeeping gene 18S or the actin mRNA and calculated using the comparative threshold cycle method ($2-\Delta\Delta^{Ct}$).

Genotoxic stimuli. For culture under stress conditions, purified splenic B cells were incubated at 37°C in RPMI-1640 containing 10% FCS in the presence or absence of etoposide (Sigma-Aldrich) or dexamethasone (Sigma-Aldrich) at the concentrations indicated in the figures. Alternatively, cells were subjected to 5 Gy γ-irradiation for the times indicated in the figures. MEFs were cultured at 37°C in DME containing 10% FCS in the presence or absence of 1 μM Dox (Sigma-Aldrich) for the times indicated in the figures. Proteins were analyzed by immunoblotting as described in Immunoblotting and immunoprecipitation. For apoptosis assays, purified splenic B cells were cultured for 20–24 h with the concentrations of etoposide indicated in the Figures. Cells were harvested and stained with Annexin V plus propidium iodide and analyzed by flow cytometry using a standard protocol.

Statistical analyses. The Student's *t* test with tail 1 and type 3 was used for statistical analyses. Values are expressed as the mean ± SD. For statistical significance: *, $P < 0.05$; **, $P < 0.005$; ***, $P < 0.0005$.

We thank A. Berns for floxed *p53* mice; the Princess Margaret Hospital/Ontario Cancer Institute Flow Cytometry Facility for cell sorting; the Campbell Family Institute for Cancer Research PCR Genotyping Facility for genotyping; and M. Saunders for scientific editing.

This work was supported by grants to T.W. Mak and Z. Hao by the Canadian Institutes of Health Research. This research was also funded in part by the Ontario Ministry of Health and Long Term Care. The views expressed do not necessarily reflect those of the Ontario Ministry of Health and Long Term Care.

The authors declare that they have no competing financial interests.

Submitted: 4 July 2011
Accepted: 17 November 2011

REFERENCES

Adhikary, S., F. Marinoni, A. Hock, E. Hulleman, N. Popov, R. Beier, S. Bernard, M. Quarto, M. Capra, S. Goettig, et al. 2005. The ubiquitin ligase HectH9 regulates transcriptional activation by Myc and is essential for tumor cell proliferation. *Cell*. 123:409–421. http://dx.doi.org/10.1016/j.cell.2005.08.016

Banin, S., L. Moyal, S. Shieh, Y. Taya, C.W. Anderson, L. Chessa, N.I. Smorodinsky, C. Prives, Y. Reiss, Y. Shiloh, and Y. Ziv. 1998. Enhanced phosphorylation of p53 by ATM in response to DNA damage. *Science*. 281:1674–1677. http://dx.doi.org/10.1126/science.281.5383.1674

Bouillet, P., D. Metcalf, D.C. Huang, D.M. Tarlinton, T.W. Kay, F. Köntgen, J.M. Adams, and A. Strasser. 1999. Proapoptotic Bcl-2 relative Bim required for certain apoptotic responses, leukocyte homeostasis, and to preclude autoimmunity. *Science*. 286:1735–1738. http://dx.doi.org/10.1126/science.286.5445.1735

Bredemeyer, A.L., G.G. Sharma, C.Y. Huang, B.A. Helmink, L.M. Walker, K.C. Khor, B. Nuskey, K.E. Sullivan, T.K. Pandita, C.H. Bassing, and B.P. Sleckman. 2006. ATM stabilizes DNA double-strand-break complexes during V(D)J recombination. *Nature*. 442:466–470. http://dx.doi.org/10.1038/nature04866

Brooks, C.L., and W. Gu. 2003. Ubiquitination, phosphorylation and acetylation: the molecular basis for p53 regulation. *Curr. Opin. Cell Biol.* 15:164–171. http://dx.doi.org/10.1016/S0955-0674(03)00003-6

Brooks, C.L., and W. Gu. 2006. p53 ubiquitination: Mdm2 and beyond. *Mol. Cell*. 21:307–315. http://dx.doi.org/10.1016/j.molcel.2006.01.020

Canman, C.E., D.S. Lim, K.A. Cimprich, Y. Taya, K. Tamai, K. Sakaguchi, E. Appella, M.B. Kastan, and J.D. Siliciano. 1998. Activation of the ATM kinase by ionizing radiation and phosphorylation of p53. *Science*. 281:1677–1679. http://dx.doi.org/10.1126/science.281.5383.1677

Chen, D., N. Kon, M. Li, W. Zhang, J. Qin, and W. Gu. 2005. ARF-BP1/Mule is a critical mediator of the ARF tumor suppressor. *Cell*. 121:1071–1083. http://dx.doi.org/10.1016/j.cell.2005.03.037

Cortez, D., Y. Wang, J. Qin, and S.J. Elledge. 1999. Requirement of ATM-dependent phosphorylation of brca1 in the DNA damage response to double-strand breaks. *Science*. 286:1162–1166. http://dx.doi.org/10.1126/science.286.5442.1162

Green, D.R., and G. Kroemer. 2009. Cytoplasmic functions of the tumour suppressor p53. *Nature*. 458:1127–1130. http://dx.doi.org/10.1038/nature07986

Hall, J.R., E. Kow, K.R. Nevis, C.K. Lu, K.S. Luce, Q. Zhong, and J.G. Cook. 2007. Cdc6 stability is regulated by the Huwe1 ubiquitin ligase after DNA damage. *Mol. Biol. Cell*. 18:3340–3350. http://dx.doi.org/10.1091/mbc.E07-02-0173

Hangartner, L., R.M. Zinkernagel, and H. Hengartner. 2006. Antiviral antibody responses: the two extremes of a wide spectrum. *Nat. Rev. Immunol.* 6:231–243. http://dx.doi.org/10.1038/nri1783

Hao, Z., and K. Rajewsky. 2001. Homeostasis of peripheral B cells in the absence of B cell influx from the bone marrow. *J. Exp. Med*. 194:1151–1164. http://dx.doi.org/10.1084/jem.194.8.1151

Hao, Z., G.S. Duncan, C.C. Chang, A. Elia, M. Fang, A. Wakeham, H. Okada, T. Calzascia, Y. Jang, A. You-Ten, et al. 2005. Specific ablation of the apoptotic functions of cytochrome C reveals a differential requirement for cytochrome C and Apaf-1 in apoptosis. *Cell*. 121:579–591. http://dx.doi.org/10.1016/j.cell.2005.03.016

Hao, Z., G.S. Duncan, J. Seagal, Y.W. Su, C. Hong, J. Haight, N.J. Chen, A. Elia, A. Wakeham, W.Y. Li, et al. 2008. Fas receptor expression in germinal-center B cells is essential for T and B lymphocyte homeostasis. *Immunity*. 29:615–627. http://dx.doi.org/10.1016/j.immuni.2008.07.016

Herold, S., A. Hock, B. Herkert, K. Berns, J. Mullenders, R. Beijersbergen, R. Bernards, and M. Eilers. 2008. Miz1 and HectH9 regulate the stability of the checkpoint protein, TopBP1. *EMBO J.* 27:2851–2861. http://dx.doi.org/10.1038/emboj.2008.200

Herzenberg, L.A. 2000. B-1 cells: the lineage question revisited. *Immunol. Rev.* 175:9–22. http://dx.doi.org/10.1111/j.1600-065X.2000.imr017520.x

Hobeika, E., S. Thiemann, B. Storch, H. Jumaa, P.J. Nielsen, R. Pelanda, and M. Reth. 2006. Testing gene function early in the B cell lineage in mb1-cre mice. *Proc. Natl. Acad. Sci. USA*. 103:13789–13794. http://dx.doi.org/10.1073/pnas.0605944103

Hodgkin, P.D., J.H. Lee, and A.B. Lyons. 1996. B cell differentiation and isotype switching is related to division cycle number. *J. Exp. Med*. 184:277–281. http://dx.doi.org/10.1084/jem.184.1.277

Jonkers, J., R. Meuwissen, H. van der Gulden, H. Peterse, M. van der Valk, and A. Berns. 2001. Synergistic tumor suppressor activity of BRCA2 and p53 in a conditional mouse model for breast cancer. *Nat. Genet.* 29:418–425. http://dx.doi.org/10.1038/ng747

Junt, T., H. Nakano, T. Dumrese, T. Kakiuchi, B. Odermatt, R.M. Zinkernagel, H. Hengartner, and B. Ludewig. 2002. Antiviral immune responses in the absence of organized lymphoid T cell zones in plt/plt mice. *J. Immunol.* 168:6032–6040.

Khanna, K.K., K.E. Keating, S. Kozlov, S. Scott, M. Gatei, K. Hobson, Y. Taya, B. Gabrielli, D. Chan, S.P. Lees-Miller, and M.F. Lavin. 1998. ATM associates with and phosphorylates p53: mapping the region of interaction. *Nat. Genet.* 20:398–400. http://dx.doi.org/10.1038/3882

Kurosaki, T., and M. Hikida. 2009. Tyrosine kinases and their substrates in B lymphocytes. *Immunol. Rev.* 228:132–148. http://dx.doi.org/10.1111/j.1600-065X.2008.00748.x

Lavin, M.F. 2008. Ataxia-telangiectasia: from a rare disorder to a paradigm for cell signalling and cancer. *Nat. Rev. Mol. Cell Biol.* 9:759–769. http://dx.doi.org/10.1038/nrm2514

Liu, Y.C., J. Penninger, and M. Karin. 2005a. Immunity by ubiquitylation: a reversible process of modification. *Nat. Rev. Immunol.* 5:941–952. http://dx.doi.org/10.1038/nri1731

Liu, Z., R. Oughtred, and S.S. Wing. 2005b. Characterization of E3Histone, a novel testis ubiquitin protein ligase which ubiquitinates histones. *Mol. Cell. Biol.* 25:2819–2831. http://dx.doi.org/10.1128/MCB.25.7.2819-2831.2005

Lumsden, J.M., T. McCarty, L.K. Petiniot, R. Shen, C. Barlow, T.A. Wynn, H.C. Morse III, P.J. Gearhart, A. Wynshaw-Boris, E.E. Max, and R.J. Hodes. 2004. Immunoglobulin class switch recombination is impaired in Atm-deficient mice. *J. Exp. Med*. 200:1111–1121. http://dx.doi.org/10.1084/jem.20041074

Matsuoka, S., B.A. Ballif, A. Smogorzewska, E.R. McDonald III, K.E. Hurov, J. Luo, C.E. Bakalarski, Z. Zhao, N. Solimini, Y. Lerenthal, et al. 2007. ATM and ATR substrate analysis reveals extensive protein networks responsive to DNA damage. *Science*. 316:1160–1166. http://dx.doi.org/10.1126/science.1140321

Meek, D.W., and C.W. Anderson. 2009. Posttranslational modification of p53: cooperative integrators of function. *Cold Spring Harb. Perspect. Biol.* 1:a000950. http://dx.doi.org/10.1101/cshperspect.a000950

Mu, J.J., Y. Wang, H. Luo, M. Leng, J. Zhang, T. Yang, D. Besusso, S.Y. Jung, and J. Qin. 2007. A proteomic analysis of ataxia telangiectasia-mutated (ATM)/ATM-Rad3-related (ATR) substrates identifies the ubiquitin-proteasome system as a regulator for DNA damage checkpoints. *J. Biol. Chem.* 282:17330–17334. http://dx.doi.org/10.1074/jbc.C700079200

Murray-Zmijewski, F., E.A. Slee, and X. Lu. 2008. A complex barcode underlies the heterogeneous response of p53 to stress. *Nat. Rev. Mol. Cell Biol.* 9:702–712. http://dx.doi.org/10.1038/nrm2451

Parsons, J.L., P.S. Tait, D. Finch, I.I. Dianova, M.J. Edelmann, S.V. Khoronenkova, B.M. Kessler, R.A. Sharma, W.G. McKenna, and G.L. Dianov. 2009. Ubiquitin ligase ARF-BP1/Mule modulates base excision repair. *EMBO J.* 28:3207–3215. http://dx.doi.org/10.1038/emboj.2009.243

Peitz, M., K. Pfannkuche, K. Rajewsky, and F. Edenhofer. 2002. Ability of the hydrophobic FGF and basic TAT peptides to promote cellular

uptake of recombinant Cre recombinase: a tool for efficient genetic engineering of mammalian genomes. *Proc. Natl. Acad. Sci. USA*. 99:4489–4494. http://dx.doi.org/10.1073/pnas.032068699

Rathmell, J.C., and C.B. Thompson. 2002. Pathways of apoptosis in lymphocyte development, homeostasis, and disease. *Cell*. 109:S97–S107. http://dx.doi.org/10.1016/S0092-8674(02)00704-3

Rathmell, J.C., T. Lindsten, W.X. Zong, R.M. Cinalli, and C.B. Thompson. 2002. Deficiency in Bak and Bax perturbs thymic selection and lymphoid homeostasis. *Nat. Immunol*. 3:932–939. http://dx.doi.org/10.1038/ni834

Rodríguez, C.I., F. Buchholz, J. Galloway, R. Sequerra, J. Kasper, R. Ayala, A.F. Stewart, and S.M. Dymecki. 2000. High-efficiency deleter mice show that FLPe is an alternative to Cre-loxP. *Nat. Genet*. 25:139–140. http://dx.doi.org/10.1038/75973

Schmidt-Supprian, M., and K. Rajewsky. 2007. Vagaries of conditional gene targeting. *Nat. Immunol*. 8:665–668. http://dx.doi.org/10.1038/ni0707-665

Schwenk, F., U. Baron, and K. Rajewsky. 1995. A cre-transgenic mouse strain for the ubiquitous deletion of loxP-flanked gene segments including deletion in germ cells. *Nucleic Acids Res*. 23:5080–5081. http://dx.doi.org/10.1093/nar/23.24.5080

Stavnezer, J., J.E. Guikema, and C.E. Schrader. 2008. Mechanism and regulation of class switch recombination. *Annu. Rev. Immunol*. 26:261–292. http://dx.doi.org/10.1146/annurev.immunol.26.021607.090248

Villunger, A., E.M. Michalak, L. Coultas, F. Müllauer, G. Böck, M.J. Ausserlechner, J.M. Adams, and A. Strasser. 2003. p53- and drug-induced apoptotic responses mediated by BH3-only proteins puma and noxa. *Science*. 302:1036–1038. http://dx.doi.org/10.1126/science.1090072

Xu, Y., T. Ashley, E.E. Brainerd, R.T. Bronson, M.S. Meyn, and D. Baltimore. 1996. Targeted disruption of ATM leads to growth retardation, chromosomal fragmentation during meiosis, immune defects, and thymic lymphoma. *Genes Dev*. 10:2411–2422. http://dx.doi.org/10.1101/gad.10.19.2411

Yin, L., S. Joshi, N. Wu, X. Tong, and M.A. Lazar. 2010. E3 ligases Arf-bp1 and Pam mediate lithium-stimulated degradation of the circadian heme receptor Rev-erb alpha. *Proc. Natl. Acad. Sci. USA*. 107:11614–11619. http://dx.doi.org/10.1073/pnas.1000438107

Zhao, X., J.I. Heng, D. Guardavaccaro, R. Jiang, M. Pagano, F. Guillemot, A. Iavarone, and A. Lasorella. 2008. The HECT-domain ubiquitin ligase Huwe1 controls neural differentiation and proliferation by destabilizing the N-Myc oncoprotein. *Nat. Cell Biol*. 10:643–653. http://dx.doi.org/10.1038/ncb1727

Zhong, Q., W. Gao, F. Du, and X. Wang. 2005. Mule/ARF-BP1, a BH3-only E3 ubiquitin ligase, catalyzes the polyubiquitination of Mcl-1 and regulates apoptosis. *Cell*. 121:1085–1095. http://dx.doi.org/10.1016/j.cell.2005.06.009